GEOPHYSICAL RESEARCH LETTERS, VOL. 37, L05803, doi:10.1029/2009GL041375, 2010

Pan-Arctic sunphotometry during the ARCTAS-A campaign of April 2008

A. Saha,[1] N. T. O'Neill,[1] E. Eloranta,[2] R. S. Stone,[3,4] T. F. Eck,[5] S. Zidane,[1] D. Daou,[1] A. Lupu,[6] G. Lesins,[7] M. Shiobara,[8] and L. J. B. McArthur[9]

Received 14 October 2009; revised 15 December 2009; accepted 31 December 2009; published 3 March 2010.

[1] Aerosol optical depth (AOD) measurements were acquired at six Arctic sunphotometer sites during the ARCTAS-A (April, 2008) campaign. Numerous smoke events were identified and related to extensive forest and agricultural fires in eastern Russia and northern Kazakhstan/southwestern Russia respectively. An analysis of the fine (sub-micron) optical depths from the six stations indicated the presence of underlying low frequency trends which were coherent with general meteorological considerations, source information, model estimates and remote sensing information. Low frequency (diurnal) coarse-mode optical depth events were observed at a number of the stations; these singular events are likely due to ice particles whose nucleation may have been associated with the presence of smoke, or possibly dust. **Citation:** Saha, A., et al. (2010), Pan-Arctic sunphotometry during the ARCTAS-A campaign of April 2008, *Geophys. Res. Lett.*, *37*, L05803, doi:10.1029/2009GL041375.

1. Introduction

[2] Forest and agricultural fires are a major source of Arctic aerosols during spring and summer [e.g., *Tomasi et al.*, 2007]. Their influence was particularly evident in April, 2008 when the Arctic Research of the Composition of the Troposphere from Aircraft and Satellites (ARCTAS-A) field campaign was conducted [*Fuelberg et al.*, 2009]. Arctic incursions of pollution and dust aerosols have also been reported in the literature [see, e.g., *Herber et al.*, 2002; *Stone et al.*, 2007].

[3] In this paper we examine pan-Arctic aerosol dynamics using sunphotometry, supported by lidar profiles, remote sensing imagery, aerosol-dynamics models and ancillary data collected during ARCTAS-A. In particular, we are concerned with the temporal/spatial synchronicity of aerosol optical depth (AOD) data divided into its fine and coarse mode components (roughly sub- and super-micron in size). The fine mode can typically be associated with forest fire smoke and pollution aerosols while the coarse mode is an indicator of supermicron sized particulates such as dust, marine aerosols, and ice or water phase cloud particulates. The formation of cloud particulates depends, in turn on the presence of aerosols acting as nucleation centers.

2. Overview of Smoke Dynamics

[4] The major fire events which occurred during the month of April, 2008 are shown in Figure S1 of the auxiliary material.[1] The range of dates for the fire events represent the period during which Fire Locating and Modeling of Burning Emissions (FLAMBE) data indicated relatively strong emissions and for which Moderate Resolution Imaging Spectroradiometer (MODIS) imagery and Global Environmental Multiscale Air Quality (GEM-AQ) AOD simulations indicated intense plume activity (see *O'Neill et al.* [2006] for a brief description of the Canadian air quality model, GEM-AQ). Figure S1 shows two large-scale fire regions; a predominantly agricultural region in southwestern Russia/northern Kazakhstan whose most intense activity occurred from April 10 to13 and April 18–22 and a largely forested region in southeast Russia whose most intense activity occurred from April 4–7 and April 15–25.

[5] Figures 1c–1e show the general motion vectors of plumes (black arrows) which had an impact on Arctic sunphotometry superimposed on representative frames of AOD maps from the GEM-AQ model (the complete GEM-AQ animations for April 2008 can be seen in Animation S1 of the auxiliary material). Purple-colored MODIS hotspots for April 2008 are superimposed on these frames to facilitate a general appreciation of the source to plume dynamics. The motion vectors are generally consistent with monthly meteorological averages during ARCTAS (Figure 1b); the polar anti-cyclone over the North Pole, a high pressure region over the northeastern Pacific and a high pressure over western Russia, a low pressure region over eastern Russia and Alaska and the low pressure system over the North Atlantic [*Fuelberg et al.*, 2009].

[6] The first large scale smoke event (SERa) was due to surges in southeast Russian fires from April 4–7. These led to, (a) large-scale smoke plumes flowing in a northeasterly direction that, after circling clockwise about the pole, generated spectacular pan-Arctic plumes whose sunphotometry impact lasted from roughly April 10–16 and (b) large-scale smoke movement (SERb) that advected in a generally northwestern direction affecting Alaska from about April 12–14.

[1] CARTEL, Université de Sherbrooke, Sherbrooke, Quebec, Canada.
[2] Space Science and Engineering Center, University of Wisconsin-Madison, Madison, Wisconsin, USA.
[3] ESRL, NOAA, Boulder, Colorado, USA.
[4] CIRES, University of Colorado at Boulder, Boulder, Colorado, USA.
[5] NASA Goddard Space Flight Center, Greenbelt, Maryland, USA.
[6] CRESS, York University, Toronto, Ontario, Canada.
[7] Department of Physics and Atmospheric Science, Dalhousie University, Halifax, Nova Scotia, Canada.
[8] National Institute of Polar Research, Tokyo, Japan.
[9] Environment Canada, Toronto, Ontario, Canada.

0094-8276/10/2009GL041375$05.00

[1] Auxiliary materials are available in the HTML. doi:10:1029/2009GL041375.

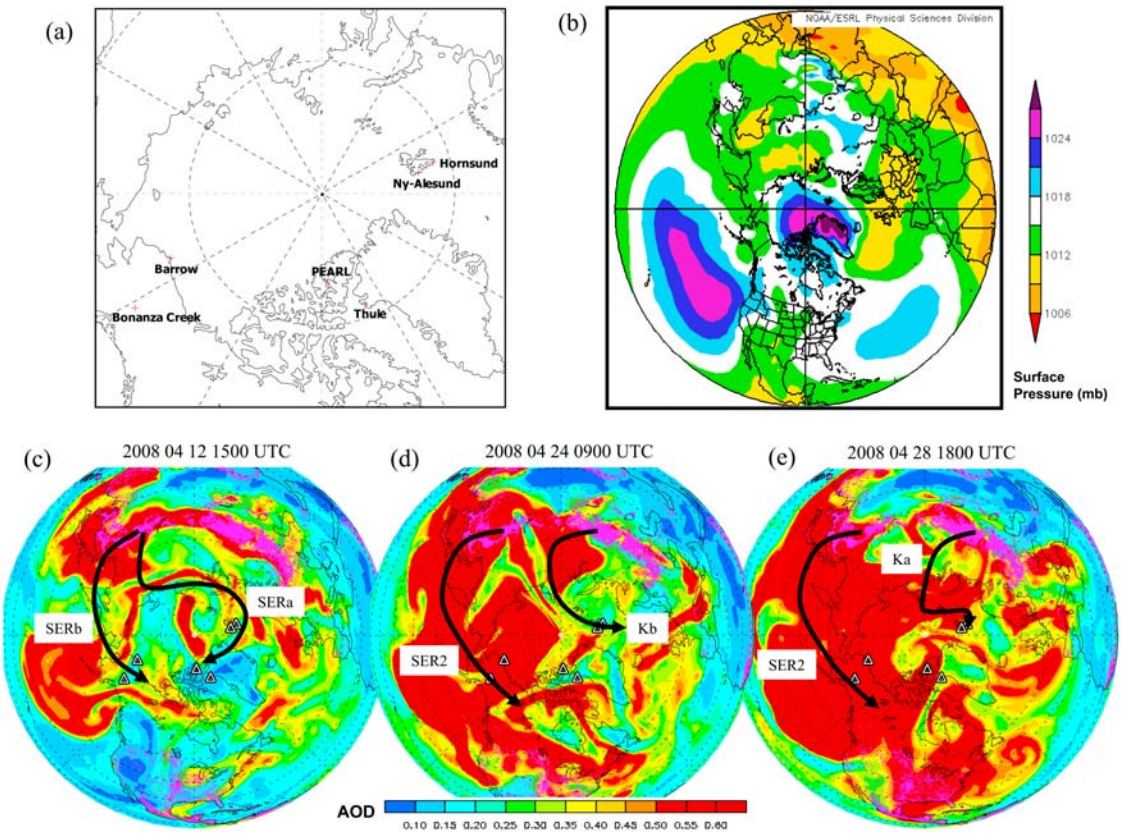

Figure 1. (a) Map of the optical sites employed in this study, (b) average surface pressure for the Arctic during April 2008, (c–e) general smoke movement schematics superimposed on representative frames of AOD estimates using the GEM-AQ model (upon which we have superimposed, in purple, the MODIS hotspot activity for April, 2008). Details on the plume labels associated with the movement vectors are given in the text while more detailed emission information associated with the labelled plumes can be seen in Figure S1.

[7] The second major series of smoke events occurred due to surges in fire activity in northern Kazakhstan and southwestern Russia from April 10–13 (primarily southwestern Russia), and in southeastern Russia from April 14–25. These fires generated large-scale plumes that affected the western Arctic and sub-Arctic region from about April 16 until the end of the month (SER2). The last large-scale smoke event that impacted Arctic sunphotometry in April was due to surges in the northern Kazakhstan and southwestern Russia region from April 19–22. These generated a northwesterly plume which affected the Arctic from at least April 22–25 (labelled Kb in Figure 1d) followed by a northeasterly movement which affected the European Arctic from at least April 28–30 (labelled Ka in Figure 1e).

3. Instrumentation and Data Processing

[8] Three lidar/sunphotometer stations were employed as our core optical sites during April, 2008; (a) The Polar Environment Atmospheric Research Laboratory (PEARL) at Eureka, Nunavut, Canada with an AEROCAN/AERONET CIMEL sunphotometer/sky radiometer (nominal λs of 340, 380, 440, 500, 675, 870, 1020 and 1640 nm) and the Arctic High Spectral Resolution Lidar (AHSRL) operating at 532 nm (brief instrument descriptions can be found in *O'Neill et al.* [2008]), (b) Barrow, Alaska, USA with a NOAA SP02 sunphotometer system (λs of 368, 412, 500, 610, 675, 778, 862 and 1050 nm) and the nearby DOE Atmospheric Radiation Measurements (ARM) micro-pulse lidar (MPL) [*Stone et al.*, 2008] and (c) Ny-Alesund, Spitsbergen, Norway with a PREDE sunphotometer/sky radiometer (λs of 400, 500, 675, 870 and 1020 nm) alongside an MPLNET (Micro Pulse Lidar NETwork) lidar operating at 523.5 nm [*Shiobara et al.*, 2008]. Figure 1a shows these sites and a second set of sunphotometer sites discussed below. The prototype MPL at Barrow provides co-polarized and cross polarized backscatter lidar ratios at 523.5 nm. All lidars, except the Ny-Alesund lidar, provide a depolarization output (depolarization ratio or cross polarization backscatter coefficient) in addition to time-height cross-sections of co-polarized backscatter coefficient. The Eureka and Ny-Alesund sunphotometers and an SP02 instrument similar to the Barrow instrument were compared and inter-calibrated, respectively, during field campaigns conducted at Ny-Alesund in April 2006 and Izana, Tennerife in October 2008. In general, AODs during the two calibration campaigns differed by $<\sim 0.005$ in the spectral range from 500 to 870 nm.

[9] Data from a second set of sunphotometer stations, without lidar support, were also analyzed to better understand Arctic-wide AOD variations. These three AERONET sites (Figure 1a) were (a) Hornsund, Spitsbergen, Norway, (b) Thule, Greenland, Denmark, and (c) Bonanza Creek, Alaska, USA. While these instruments were not part of the intercalibration campaigns discussed above, they were

calibrated before and after the ARCTAS-A campaign as part of the regular AERONET calibration rotation.

[10] Our approach was to analyze pan Arctic AOD data resolved into fine and coarse mode components using a spectral deconvolution (SDA) algorithm [*O'Neill et al.*, 2008]. Briefly, we employ the measured AOD spectra to extract fine and coarse mode optical depth (τ_f and τ_c) at a reference wavelength of 500 nm. The UV (340nm), NIR (1020 or 1050 nm) and SWIR (1640 nm) channels were excluded from the SDA processing for all instruments in order to respectively, avoid the spectral influence of greater calibration uncertainty in the UV [*Eck et al.*, 2009], minimize spectral artifacts due to temperature and water vapour absorption and because the SWIR channel was not needed to extract the type of information required in the current analysis.

[11] We tried to minimize interpretative processing such as cloud screening for all stations (Level 1.0 AERONET data and non-cloudscreened data for the PREDE sunphotometer were employed). For AERONET data this means that no cloud screening was performed but that recalibration had been performed (a linear interpolation between pre and post calibration results).The non-cloudscreened Barrow data was characterized by high temporal resolution (1 second per AOD spectrum) and relatively high temporal sampling frequency (1 minute). This and other protocols generated a highly variable AOD time series compared to AEROCAN/AERONET data (whose significantly different protocols include an AOD spectrum sampling time of 8 seconds, a nominal sampling frequency of 3 minutes and pre-cloudscreening for highly variable triplet measurements). We accordingly opted to resample the Barrow data set to a 3 minute frequency and perform some simple (and fairly lenient) filtering ($\tau_c < 0.6$ and solar airmass < 8 with estimated SDA retrieval error of $\Delta\tau_f < 0.2$; this latter constraint amounting to an acknowledgetment that τ_f estimates are of little value when τ_c completely dominates the optical depth signal).

4. Sunphotometry and Lidar Results

4.1. Sample Results for Combined Lidar/Sunphotometry Stations

[12] Figure 2 shows the τ_a (total AOD), τ_f and τ_c variation aligned with AHSRL profiles of backscatter coefficient (β) and depolarization ratio (δ) for April 2008. This type of combined plot has been discussed by *O'Neill et al.* [2008]; the τ_f values are typically well correlated with β in the presence of small δ while the τ_c values correlate with β in the presence of large δ (illustrated in Figure S5 of the auxiliary material).

[13] The same type of lidar/sunphotometry overlay graphic was produced for Barrow and Ny-Alesund in order to validate our hypotheses as to the occurrence of fine or coarse mode events on any given day. This validation was supported by MODIS imagery, FLAMBE emission data, model predictions and back-trajectories in much the same manner discussed by *O'Neill et al.* [2008].

4.2. Fine Mode Events

[14] Figure 3 shows τ_a, τ_f, and τ_c time series during April for all the six sites of Figure 1a. The greyish zones and their labels indicate smoke events which we were able to identify at the three core sites given the criteria put forth in section 4.1. The solid red line is the result of a low-frequency box-car filter being applied to the τ_f time series (see Figure 3 caption for more details). MODIS and MISR imagery demonstrate the detectability of the smoke plumes near some of the sites (Figures S2–S7 of the auxiliary material).

[15] Between the SERa plumes on April 12–14 and April 16 and the Kb plume of April 24 one can observe an apparent low frequency increase in τ_f over the Eureka site in Figure 3a. Between about April 15 and April 22 the polar anticyclone (Figure 1b) was largely replaced by a cyclonic low whose pressure centre descended from Spitsbergen towards Eureka and then back over Spitsbergen. Although there are no obvious plumes over Eureka in the MODIS imagery during this low pressure cyclonic event, there are clear indications of complex, low-depolarization-ratio, turbidity variations in the AHSRL profiles of Figure 2. Values of τ_f were elevated on April 22 and 23 but the fine-mode scattering effects were arguably too dispersed to be readily identified in MODIS imagery. While the time period between April 17 and 21 is largely dominated by τ_c events, there are occasional windows of 2–4 hour duration when τ_f was elevated (April 19, 20 and 21) suggesting that the elevated τ_f values estimated in Figures 2 and 3a are real. These τ_f windows are important because they yield more confidence in τ_f estimates outside the windows (the ability to predict τ_f values in the presence of larger τ_c values is largely untested).

[16] The same series of east-to-west SERa plumes which affected Eureka on April 12 and 13 affected Thule optical depths with an advective lead of ~8 hours. While the Thule graph appears to show elevated values of τ_f between April 12 to April 16 the latter three days are coarse mode dominated and this apparent trend has to be considered with this limitation in mind. These east to west advecting plumes later appeared to circle cyclonically (CCW) around the above mentioned low pressure whose descending frontal edge was north of Eureka on April 16. Thule data showed elevated values of τ_f that persisted from about April 12 to the end of the month, and which were roughly similar, in their general, low-frequency trend, with the temporal profile of the Eureka τ_f values.

[17] MODIS imagery and HYSPLIT trajectories suggest that the strong plume that affected Eureka on April 12 and which was the leading edge of the SERa series of plumes passed over Ny-Alesund on April 10 (the grey zone labelled "SERa" on Figure 3c). While it was very cloudy at Ny-Alesund on April 10, the MPLNET lidar did see 5–8 km altitude plume structure (over a narrow time window) that roughly matched the altitude range of the April 12 plume over Eureka. Later in the month, the Kb and Ka plumes contributed to substantial increases in the fine mode at Ny-Alesund (grey zones labelled "Kb" and "Ka" on Figure 3c). MODIS imagery and HYSPLIT trajectories indicate that the Kb plumes actually split into an eastern branch between 3 and 5 km altitude that advected over Ny-Alesund on April 24 and 25 and a western branch at approximately 5 km that reached Eureka on April 24. In general, the Ny-Alesund τ_f values remain relatively high between the start and end of the PREDE measurements (April 9–29).

[18] The lack of obvious correlation between Hornsund and Ny-Alesund, two relatively close stations (230 km separation), is partly attributable to data gaps which appear in Ny-Alesund as well as Hornsund data and partly attributable to the complex meteorology of the Spitsbergen region.

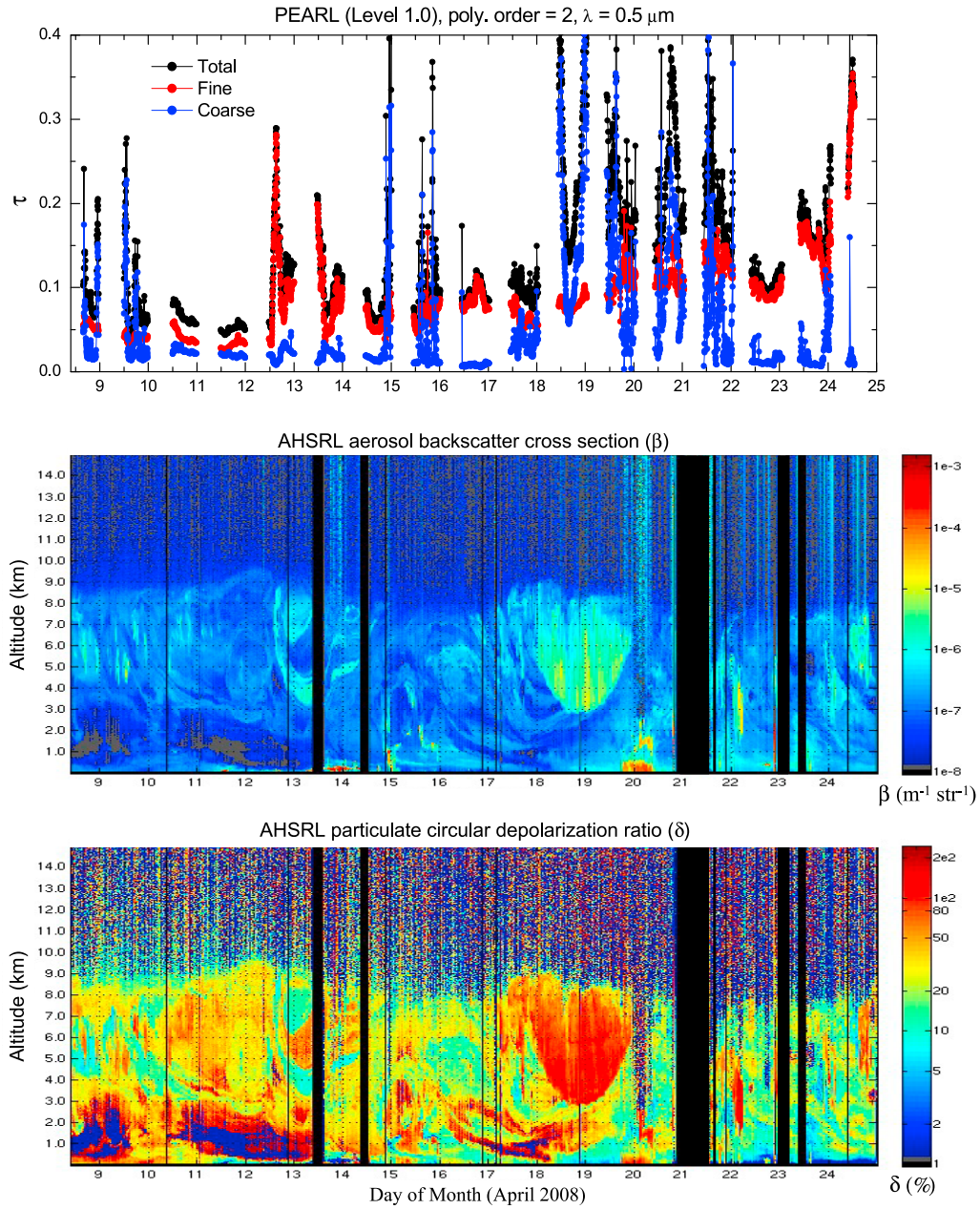

Figure 2. τ_a or total AOD (black) τ_f (red) and τ_c (blue) (500 nm) retrievals at PEARL, lined up with 532 nm AHSRL profiles of β and δ.

The peak values of τ_f observed between April 23 and 30 at Hornsund were, except for April 29, associated with large τ_c. However there were short time windows in the Hornsund data which were fine mode dominated; the continuity across τ_f dominated/τ_c dominated boundaries lent confidence to τ_f predictions in the presence of large τ_c and thus the general form of the filtered τ_f curve.

[19] Barrow was affected by frequent smoke plumes during April of 2008 [see, e.g., *Warneke et al.*, 2009]. Figure 3e shows the identified smoke plumes for the SERb and SER2 cases at Barrow. From about April 13 to the end of the month, one observes a general increase in τ_f which could be characterized as being convolved with higher frequency variations associated with specific smoke events. The Bonanza Creek low frequency variations in τ_f appear to increase during roughly the same period but are not influenced by an event analogous to the strong fine mode event of April 19 at Barrow. This is arguably the biggest difference between the two curves; *Eck et al.* [2009] show very similar results (including the disparity on April 19) when they argue that the low frequency (daily averaged) AOD (500 nm) statistics for Barrow and Bonanza Creek during April 2008 were very similar.

4.3. Coarse Mode Events

[20] Figure 2 shows a high δ event on April 18 and 19 for which τ_c varied in a low frequency (diurnal) fashion (unlike typical cloud effects whose high frequency τ_c excursions form the basis of most cloud screening algorithms). The AHSRL profiles of April 17 pm showed a more balanced

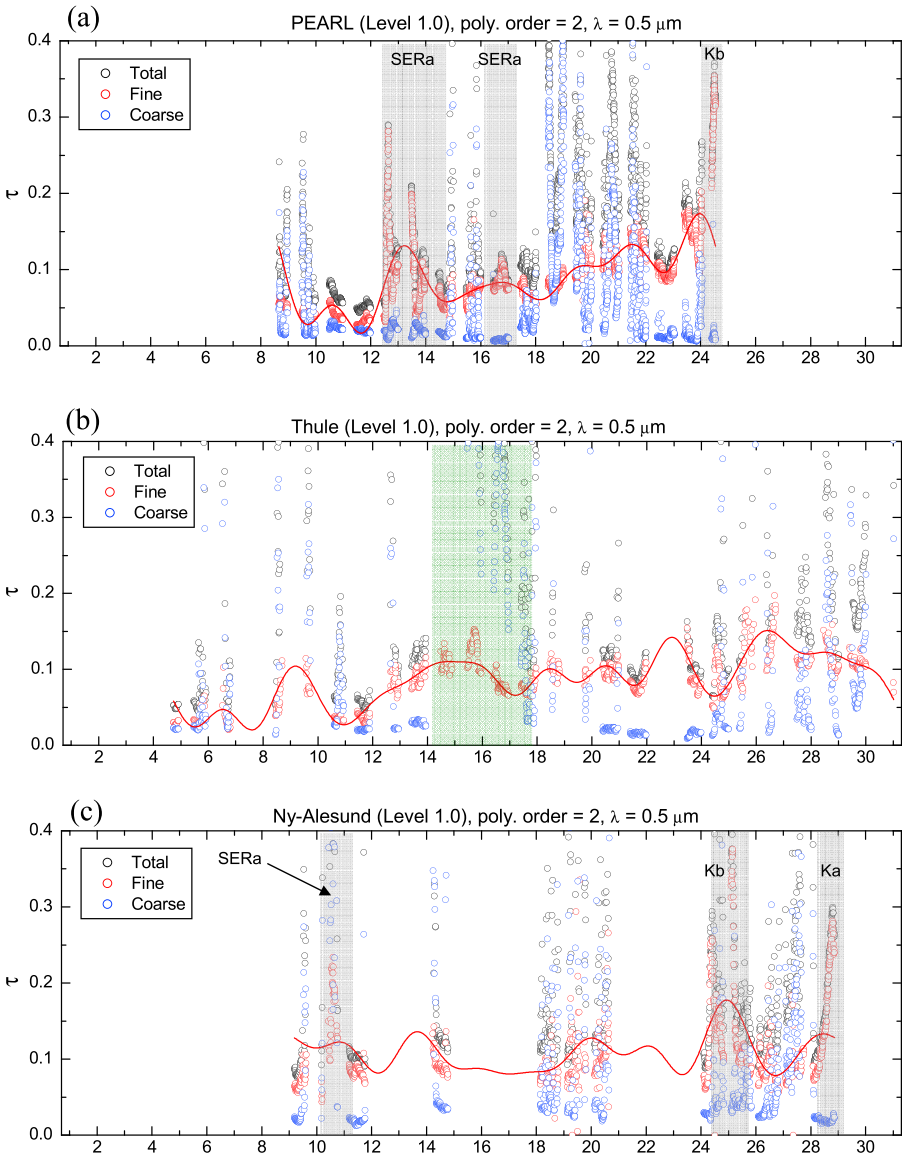

Figure 3. τ_a, τ_f and τ_c (500 nm) retrievals at the six sunphotometer stations of Figure 1: (a) PEARL, (b) Thule, (c) Ny-Alesund, (d) Hornsund, (e) Barrow, and (f) Bonanza Creek. The grey areas represent confirmed cases of smoke while the labels indicate the source of the smoke (cf. Figure S1). The solid red line represents the results of a box-car frequency filter applied to τ_f (maximum frequency = 1/2 cycle per day). The green area shows the period when the Thule sunphotometer suffered from window frosting.

mixture of high-δ structure over a low-δ feature which was visually coherent with the τ_f and τ_c temporal variation. MODIS images on April 18 and 19 showed plume-like structure not unlike the shadow and bright band structures which we often associated with smoke plumes (during these two days the April 15–22, polar cyclonic low mentioned above was moving north, as were the plumes observable in the MODIS imagery). The smoke plume positions inferred from MODIS imagery and April 15–22 synoptic- dynamics combined with an analysis of the lidar/sunphotometry data and AOD simulations suggest that these features were a complex mixture of smoke and ice crystals and that the smoke may have played a nucleation role. The aerosol assimilation studies [*Pierce*, 2009] suggest that smoke and possibly dust transported from Asia affected AODs at Eureka.

[21] The Thule site was also apparently affected by high-amplitude, low frequency τ_c variations from April 14 to 18 (green zone in Figure 3b). However, this data revealed suspicious, diurnal behaviour. In the past, similar behaviour, observed at Eureka, was attributed to optics contamination due to frost; the telltale signature being a rather symmetric, large-amplitude diurnal cycle in τ_c (associated with artifactual radiance discrepancies between sky radiance measurements acquired by the CIMEL extinction collimator and the sky radiance collimator). There were no low-frequency, elevated-τ_c events evident in the Ny-Alesund time series or at Hornsund, but a few isolated cases were noted for Barrow. One particular event over Barrow on April 9 showed significant, low-frequency τ_c variation (with one peak achieving values ~ 0.2) matched with enhanced back-

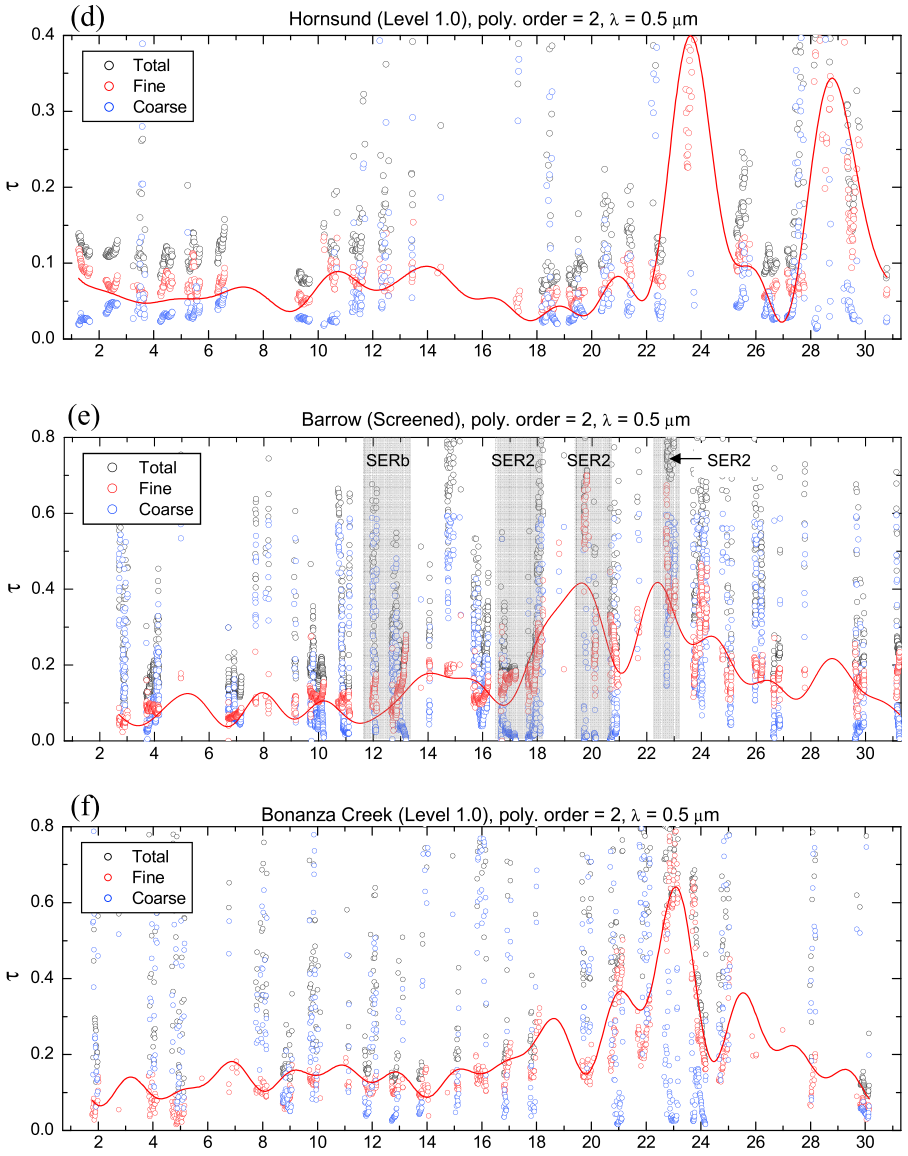

Figure 3. (continued)

scatter and high cross-polarization profiles as measured by the MPL (Figure S8). *Ferrare et al.* [2009] concluded, using airborne lidar measurements acquired near Barrow on April 9 (and other days), that ice particles were making a significant contribution to the AOD.

5. Summary and Conclusions

[22] AOD measurements acquired at six Arctic sunphotometer sites during the April, 2008 ARCTAS-A campaign were analyzed with the goal of understanding AOD contributions on a pan-Arctic scale. Prominent smoke events were identified and linked to extensive fires in eastern Russia and northern Kazakhstan/southwestern Russia, respectively. The ability to identify smoke plumes over homogeneous, brightly reflecting, Arctic ice in MODIS and MISR imagery suggests that a satellite-based, AOD inversion scheme over the Arctic is feasible. An analysis of the fine (sub-micron) optical depths from the six stations indicated the presence of low-frequency signal components which were coherent with general meteorological considerations, source information, model estimates and remote sensing information. Low frequency coarse-mode optical depth events were observed at a number of the stations; these singular events are likely due to ice particles whose nucleation may have been associated with the presence of smoke (and possibly dust).

[23] **Acknowledgments.** The authors would like to thank four Canadian agencies, NSERC, CFCAS, CFI and FQRNT (Québec) for their financial support. The authors also acknowledge NOAA-ARL (HYSPLIT), DOE/ARM (Barrow MPL data), NRL (FLAMBE) and NASA (MODIS, MISR and the AERONET project). MPLNET is funded through NASA's EOS and Atmospheric Radiation Sciences program. Valuable support was also provided by Environment Canada (EC). The contributions of Ihab Abboud (EC), M. Okraszewski, A. Khmel, and O. Mikhailov of CANDAC

are gratefully acknowledged. We also thank M. Sofiev for providing biomass burning emissions.

References

Eck, T. F., et al. (2009), Optical properties of boreal region biomass burning aerosols in Alaska and transport of smoke to arctic regions, *J. Geophys. Res.*, *114*, D11201, doi:10.1029/2008JD010870.

Ferrare, R., et al. (2009), Arctic aerosol properties derived from remote sensing measurements on the NASA B200 King Air aircraft, paper presented at the POLARCAT Workshop, Int. Global Atmos. Chem. Program, Durham, N. H., 2–5 June.

Fuelberg, H. E., D. L. Harrigan, and W. Sessions (2009), A meteorological overview of the ARCTAS 2008 mission, *Atmos. Chem. Phys. Discuss.*, *9*, 18,417–18,478.

Herber, A., L. W. Thomason, H. Gernandt, U. Leiterer, D. Nagel, K.-H. Schulz, J. Kaptur, T. Albrecht, and J. Notholt (2002), Continuous day and night aerosol optical depth observations in the Arctic between 1991 and 1999, *J. Geophys. Res.*, *107*(D10), 4097, doi:10.1029/2001JD000536.

O'Neill, N. T., et al. (2006), Evaluation of the GEM–AQ air quality model during the Québec smoke event of 2002: Analysis of extensive and intensive optical disparities, *Atmos. Environ.*, *40*(20), 3737–3749, doi:10.1016/j.atmosenv.2006.03.006.

O'Neill, N. T., O. Pancrati, K. Baibakov, E. Eloranta, R. L. Batchelor, J. Freemantle, L. J. B. McArthur, K. Strong, and R. Lindenmaier (2008), Occurrence of weak, sub-micron, tropospheric aerosol events at high Arctic latitudes, *Geophys. Res. Lett.*, *35*, L14814, doi:10.1029/2008GL033733.

Pierce, R. B. (2009), RAQMS chemical and aerosol assimilation studies during the 2008 NOAA ARCPAC field mission, paper presnted at the 6th Annual CoRP Science Symposium, NOAA, New York, N. Y., 18–19 Aug.

Shiobara, M., et al. (2008), Optical properties of arctic aerosol in spring based on sky-radiometer and micro-pulse lidar measurements at Ny-Alesund, Svalbard, paper presented at the Eighteenth Atmospheric Radiation Measurement Science Team Meeting, U.S. Dep. of Energy, Norfolk, Va.

Stone, R. S., G. P. Anderson, E. Andrews, E. G. Dutton, E. P. Shettle, and A. Berk (2007), Incursions and radiative impact of Asian dust in northern Alaska, *Geophys. Res. Lett.*, *34*, L14815, doi:10.1029/2007GL029878.

Stone, R. S., G. P. Anderson, E. P. Shettle, E. Andrews, K. Loukachine, E. G. Dutton, C. Schaaf, and M. O. Roman III (2008), Radiative impact of boreal smoke in the Arctic: Observed and modeled, *J. Geophys. Res.*, *113*, D14S16, doi:10.1029/2007JD009657.

Tomasi, C., et al. (2007), Aerosols in polar regions: A historical overview based on optical depth and in situ observations, *J. Geophys. Res.*, *112*, D16205, doi:10.1029/2007JD008432.

Warneke, C., et al. (2009), Biomass burning in Siberia and Kazakhstan as an important source for haze over the Alaskan Arctic in April 2008, *Geophys. Res. Lett.*, *36*, L02813, doi:10.1029/2008GL036194.

D. Daou, N. T. O'Neill, A. Saha, and S. Zidane, CARTEL, Université de Sherbrooke, Sherbrooke, QC J1K 2R1, Canada. (auromeet.saha@usherbrooke.ca)

T. F. Eck, NASA Goddard Space Flight Center, Code 923, Greenbelt, MD 20771, USA.

E. Eloranta, Space Science and Engineering Center, University of Wisconsin-Madison, 1225W. Dayton St., Madison, WI 53706, USA.

G. Lesins, Department of Physics and Atmospheric Science, Dalhousie University, Dunn Bldg., Halifax, NS B3H 1Z0, Canada.

A. Lupu, CRESS, York University, 4700 Keele St., Toronto, ON M3J 1P3, Canada.

L. J. B. McArthur, Environment Canada, 4905 Dufferin St., Toronto, ON M3H 5T4, Canada.

M. Shiobara, National Institute of Polar Research, 9-10 Kaga 1-chome, Itabashi-ku, Tokyo 173-8515, Japan.

R. S. Stone, CIRES, University of Colorado at Boulder, 216 UCB, Boulder, CO 80309-0216, USA.